

4-4 Development of CRL Fabry-Perot interferometers and observation of the thermosphere

ISHII Mamoru, OKANO Syoichi, SAGAWA Eiichi, MURAYAMA Yasuhiro, WATARI Shinichi, Mark Conde, and Roger W. Smith

The Fabry-Perot Interferometer (FPI) has long been established as a remarkably versatile high-resolution system for a wide range of spectroscopic purposes. This system screens out rays with a specific wavelength by letting multiple reflections occur between two glass plates called etalon. It has been used for estimating wind velocity and temperature in the mesosphere and the thermosphere which is much difficult to deduce with other observational methods. We have developed two types of FPI, the all-sky FPI and the scanning FPI as a part of international cooperative research project between CRL and University of Alaska, Fairbanks.

After several operations in Japan for improving total systems, we installed these instruments in Alaska. The scanning FPI, installed in the Poker Flat Research Range, is used for vertical wind feature in the vicinity of aurora. The all-sky FPI, installed at the Eagle observatory, is used for ionosphere - thermosphere coupling study with cooperative observations with HF-radar.

We have developed an automatic observation system for operating the instrument and data analyzing software for retrieving parameters with high precisions.

Keywords

Airglow, Aurora, Neutral wind, Thermosphere, Vertical wind

1 The Significance of Neutral-Wind and Temperature Observations in the Thermosphere Using Fabry-Perot Interferometers

Charged particles originating from the sun undergo complex interactions with the magnetosphere surrounding the Earth before reacting with the atmosphere at both poles, creating dynamic electromagnetic effects, such as auroral activity. The energies of these particles are eventually supplied to the neutral particles in the thermosphere and mesosphere as light, heat, or kinetic energy. Although models of this system^{[1][2]} exist in individual cases^[3], there has been little observation and scant

progress in the investigation of the amount of solar energy supplied to the Earth's atmosphere via these particles.

Energy is also known to be supplied to the mesosphere and the lower thermosphere from below. At the boundary layer of the mesosphere and the lower thermosphere (a boundary referred to as the "mesopause") located at an altitude of approximately 85 km, the horizontal wind speed becomes nearly zero, and the rotation of this layer is nearly synchronous with the ground surface. This is a strange phenomena, considering that horizontal winds of velocities exceeding 50 m/s are constantly present between the ground and the mesopause. Presently, this phenomenon is explained in terms of the breaking of gravity

waves propagating from below[4]. However, a quantitative investigation of this mechanism through wide, long-term observation has yet to be undertaken.

Climate changes such as those associated with global warming are thought to be related to this energy balance in the mesosphere and thermosphere, the importance of which is becoming increasingly recognized. However, direct observation of this region using satellites or radiosonde is difficult; remote sensing using radio waves and light is considered to be more effective in continuous observation of this region.

The ultra upper atmosphere constantly emits a faint light, both during the day and at night. This emission is caused by photoionization and photodissociation by sunlight and by the collisions between the particles themselves. This phenomenon, known as “air-glow”, consists of light at a specific wavelength. When this emission is measured at highly precise wavelength resolutions, the velocity of the radial motion of the air (i.e., the wind) producing the glow can be deduced from the shift between predicted and observed wavelengths, and the temperature of the air can be estimated from the spectral wavelength width. Auroras seen in polar regions are produced by the excitation of the atmosphere by precipitation of high-energy particles from the solar wind along the magnetic line of force of the Earth. Although the mechanism of luminance differs between the aurora and the air-glow, common spectrometric methods may be used to observe both phenomena, as they both represent atmospheric emissions at a specific wavelength.

As part of a cooperative research project with the University of Alaska Fairbanks (UAF), the Communications Research Laboratory (CRL) has developed the Fabry-Perot interferometers (FPI). These instruments use a pair of glass plates in a configuration referred to as an “etalon” to cause multiple reflections and interference patterns of light in order to screen out rays of a specific wavelength with extremely high resolution. One of

the goal of the Alaska Project is to conduct an study of the interaction of the ionosphere and thermosphere in the polar regions; in this context optical observation using FPI is expected to provide a valuable means of understanding thermospheric dynamics.

In this paper, the principles of FPI observation and the FPI program developed by the CRL (CRLFPI) will be presented, as well as some of the results of observations using this FPI.

2 Principles of Observation with a Fabry-Perot Interferometer

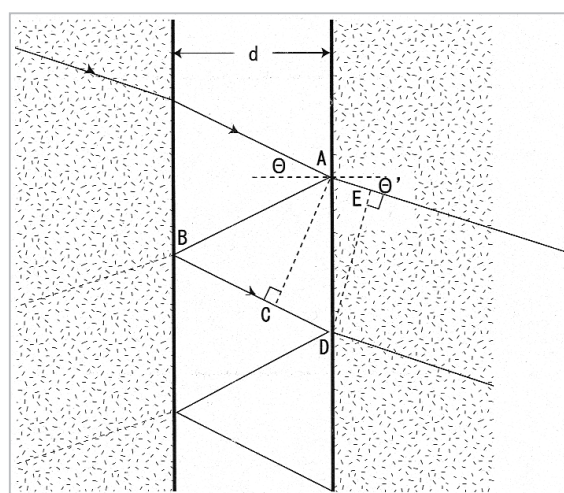


Fig.1 Schematic diagram of etalon

Light rays entering from the upper left undergo multiple reflections between two mirrors facing each other and create interference as they exit at the right.

Fig.1 shows a schematic diagram of the optical device known as the etalon, which forms the core element of the Fabry-Perot interferometer. Two glass plates with mirrored surfaces specially coated to produce a reflectance of approximately 90% are placed facing each other, in a precisely parallel position set using piezo actuators or high-precision screw heads. As shown in Fig. 1, when light enters the two parallel glass plates (refractive index n' , where $n' > n$) placed a distance d apart in a medium with a refractive index of n at an incidence angle of θ , the optical-path difference is $CD \cdot n = AE \cdot n'$, which can be expressed as $AB + BC = 2nd \cos \theta$. For light

with wavelength λ , the phase difference between the primary (reflected 0 times) and secondary (reflected once) emerging light can be expressed as

$$\phi = 2\pi/\lambda \cdot 2nd \cos \Theta = 4\pi nd \cos \Theta / \lambda \quad (1)$$

Here, the distance is normalized to the amplitude of the incidence angle. When the amplitude transmittance of the reflective membrane of the etalon plate is t , the amplitude reflectance is $r \cdot \exp(i\chi)$, and the phase change upon reflection is χ . Therefore, the amplitude of the light ejected from the interferometer can be expressed as

$$\begin{aligned} \tau &= t^2 + t^2(r \cdot \exp(i\chi))^2 \cdot \exp(i\phi) + t^2(r \cdot \exp(i\chi))^4 \cdot \exp(2i\phi) + \dots \\ &= t^2 / (1 - r^2 \exp(i(\phi + 2\chi))) \end{aligned} \quad (2)$$

If the intensity transmittance of the reflector membrane of the etalon plate is T , and the intensity reflectance is R , then $T = t^2$, $R = r^2$. When $\chi = \pi/2$,

$$\tau = T / (1 - R \cdot \exp(i\delta)) \quad (3)$$

Since the intensity transmittance of the entire etalon T_{FP} can be expressed as the square of the absolute amplitude transmittance, or $T_{FP} = |\tau|^2$,

$$T_{FP} = T^2 / (1 + R^2 - 2R \cos \delta) \quad (4)$$

When the light reflected from both plates is in phase, or when $\delta = 2m\pi$ ($m = 0, \pm 1, \pm 2, \dots$), the intensity transmittance of light will be maximum ($T_{FP} = 1$), and when $\delta = (2m + 1)\pi$, T_{FP} will be minimum. If the surface area of the light source is sufficiently large, then the parts illuminated on the focal plane at maximum transmittance will form concentric ring patterns, as shown in Fig.2. These rings are called fringes, and their intensity cross-section follows the function given by Equation (4), known as the Airy function.

Equation (4) is a function of δ , so it will be converted into a function of distance a from the center or the fringe, which will actually appear on the CCD camera. By Taylor expansion of Equation (1), we obtain

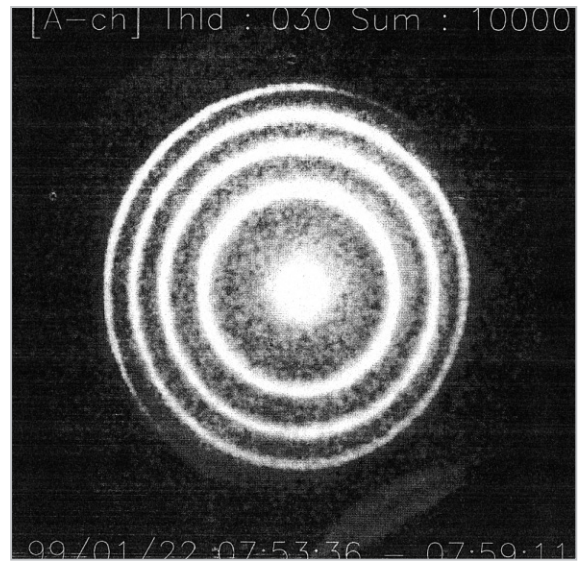


Fig.2 An example of a laser fringe actually observed by the CRLFPI (wavelength 623.7 nm; integrated 10,000 times)

$$\phi = \frac{4\pi nd}{\lambda} \left(1 - \frac{\Theta^2}{2!} + \frac{\Theta^4}{4!} - \dots \right) \quad (5)$$

When $\Theta \cong 0$, then $\Theta \cong \tan \Theta = a/f$. Using this relationship, we obtain

$$\phi = \frac{4\pi nd}{\lambda} \left(1 - \frac{a^2}{2f^2} + \frac{a^4}{24f^4} - \dots \right) \quad (6)$$

where a is the distance from the fringe center and f is the focal distance from the focus lens. Since $a \ll f$, the third term can be ignored. Inserting this result into Equation (4), we obtain

$$T_{FP} = \frac{T^2}{1 + R^2 - 2R \cos \left(\frac{4\pi nd}{\lambda} \left(1 - \frac{a^2}{2f^2} \right) + 2\chi \right)} \quad (7)$$

If the air emitting the observed airglow is moving in the radial direction, the Doppler effect will shift the wavelength of the airglow, and this in turn will shift the peak position of the fringe. Further, an increase in the air temperature will cause the width of the fringe to increase. Therefore, information about the wind speed and air temperature can be obtained by calculating the changes in the fringe position and width based on the standard position and width.

Fig.3 shows the relationship between the wavelength of the incident light and the fringe peak position, when the etalon gap $d = 20.49$ mm, space permeability $\mu = 4 \times 10^{-7}$, and $f = 0.6$ m. The right vertical axis represents the motion of the luminescent body (in this case, wind speed) calculated from the Doppler shift at an incident wavelength of 557.7 nm. This presentation, using a as the parameter, is called the R-space. However, the relationship presented here is not linear; in other words, as the fringe radius increases, the change caused by the same wind speed will be smaller. A linear relation can be obtained by using a^2 as the parameter instead of a , as in Fig. 4, which shows the relationship between the wavelength of the incident light and the fringe peak position. The parameters and vertical axis are the same as those in Fig.3.

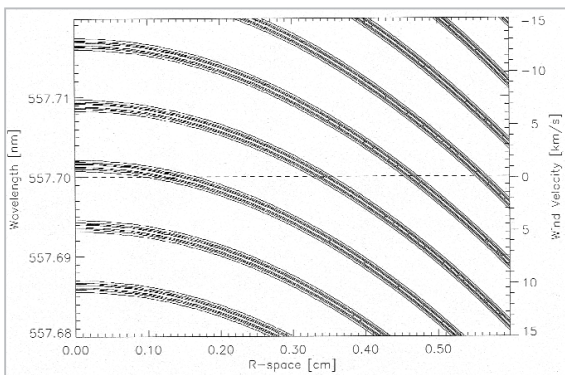


Fig.3 Correlation between the wavelength of the incident light and the position of the fringe peak in R-space

The horizontal and vertical axes represent fringe radius and wavelength, respectively. Here, the etalon gap is set as $d = 20.49$ nm, space permeability $\mu = 4 \times 10^{-7}$, and $f = 0.6$ m. The right vertical axis represents the motion of the luminescent body (in this case, wind speed) calculated from the Doppler shift at an incident wavelength of 557.7 nm.

When detecting the temperature, the fringe cross-section of the laser is used to determine the instrumental function. If we assume that the wavelength of the laser beam is ideally uniform, the spectral width of the laser will not be affected by temperature, and so the measured airglow can be considered to have been emitted from air at a temperature of 0 K. The fringe pattern created by a laser beam can

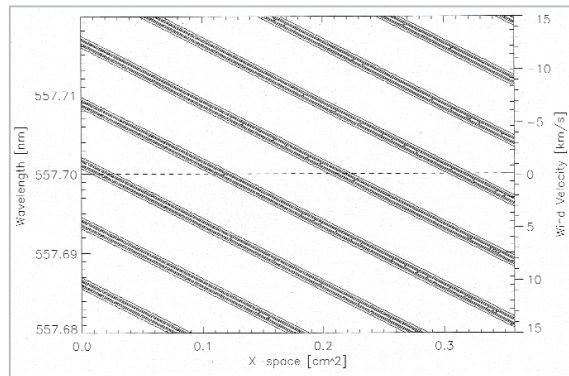


Fig.4 Correlation between the wavelength of the incident light and the position of the fringe peak in X-space

Notation is the same as in Fig.3.

be represented by Equation (7); this pattern is dependent only on instrumental parameters. In comparison, observations of actual airglows will reveal temperature-dependent spectral widths, and so the fringe patterns will represent a convolution of the temperature distribution and the instrumental functions. Thus, the atmospheric temperature will be able to be determined by deconvolution of the airglow fringe using the instrumental functions.

Equation (7) represents an instrumental function for an ideal etalon. With actual etalons, factors such as microscopic defects of the mirror surface, imperfections in flatness, and finite etalon diameter must be taken into consideration. The spatial resolution of the detector is also an important factor.

See [5] and [6] for more details on the theory of Fabry-Perot interferometers.

3 Scheme of the CRLFPI

3.1 Optical System

There are currently two types of Fabry-Perot interferometers: the scanning FPI and the all-sky FPI, categorized based on their respective pre-optical systems (preceding the etalon). Scanning FPI has been in use for a long time, to perform observations of a relatively limited region of the sky using mirrors and the like. The all-sky FPI uses a fish-eye lens to make observations of the entire sky at once. One model of each type was developed for the CRLFPI for the purpose of performing

measurements of thermospheric dynamics in the vicinity of auroras with large temporal variations. Fig.5 represents a schematic diagram of the CRLFPI optical system. (For details on the instruments, see [7] and [8].)

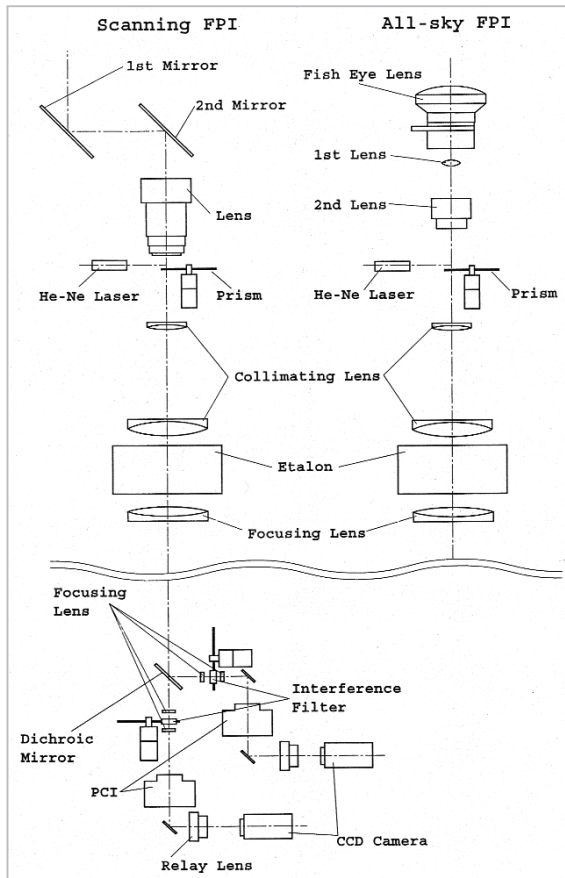


Fig.5 The CRLFPI optical system

Left: scanning FPI; Right: all-sky FPI. Rear optical systems (positioned behind the etalon) are common.

Since airglows feature extremely low luminous energy, their signals must be multiplied electronically. In contrast, auroras feature relatively high levels of luminous energy, but they are also subject to marked temporal variations, and so a high temporal resolution is required during observation. Therefore, the CRLFPI uses a Photon Counting Imager (PHI; Hamamatsu Photonics K.K.) for multiplication.

One of the characteristic of the CRLFPI is that it uses dichroic mirrors to perform simultaneous observations at two wavelengths, which means that it is capable of making

observations of wind speed and temperature simultaneously, at altitudes corresponding to two different airglow regions.

Generally, airglow is observed with an FPI using the atomic oxygen line at 557.7 nm and 630.0 nm. In recent years, improvements in detector sensitivity have made it possible to observe OH emissions (at 843.0 nm, for example). Measurements at wavelengths of 557.7 nm (with a peak altitude at approx. 95 km for airglow and at approx. 110 km for auroras) and 843.0 nm (approx. 86 km) are effective for estimation of the wind velocity and temperature in the lower thermosphere and mesosphere, and measurement at 630.0 nm (approx. 250 km) is effective for the F region in the ionosphere, located above.

The CRLFPI has been moved to Alaska, U.S., along with various control systems, which will be discussed in later sections. The scanning FPI has been installed at the Poker Flat Research Range of the UAF (65.12°N, 147.43°W), and the all-sky FPI has been installed at the Eagle Observatory (64.78°N, 141.16°W).

3.2 Data Retrieval System

Fig.6 represents a schematic diagram of the CRLFPI systems (other than the optical system), consisting of the data-processing system for the acquisition of fringe images as digital data and their storage within workstations, a drive/control system for the motors, a housekeeping system to maintain the required observation conditions, and an automatic observation system for conducting continuous, long-term, unmanned observations lasting several months.

The data-retrieval system consists of a CCD camera (Hamamatsu Photonics VH5200), an image processor (Image Systems Co., Ltd.), and a workstation to control image retrieval and data storage (Sun Microsystems, Inc.). The CCD camera acquires images at a video rate of 30 images/sec., and sends them to the image processor, where A/D conversion is performed, along with integration. The threshold and the number of images integrated

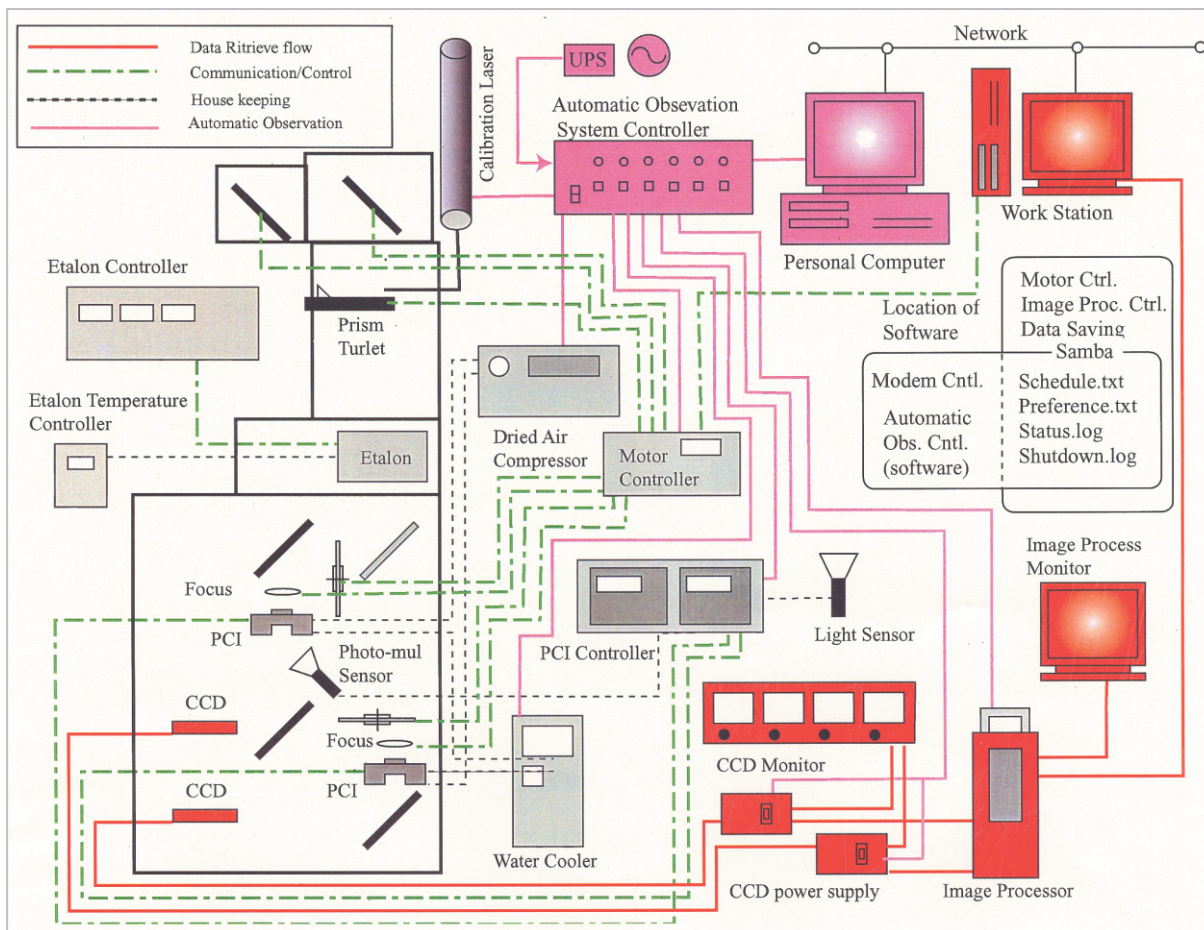


Fig.6 Schematic diagram of the CRLFPI systems (other than the optical system)

The instruments shown in red, green, black, and pink represent the data-retrieval, drive/control, house-keeping, and automatic observation systems, respectively.

in the A/D conversion are set within the workstation environment. The integrated digital images are then sent to the workstation, where they are stored. The data size for a single channel is approximately 492 KB for a binary image of 512×480 pixels at 16 bits/pixel and a header of 128 bytes. Normally, observation is performed using two channels, in which case the header will be shared, so the data size will be approximately 983 KB. The observation time will depend upon the brightness of the airglow and the performance of the optical system, but it has been empirically confirmed that for auroras, an integration of two minutes will produce a sufficiently high S/N ratio in terms of analysis. In cases of observations where luminance is insufficient, it is possible to improve the S/N ratio through digital summing of multiple images.

In the Alaska Project, a data-archiving system (the SALMON system) is being developed for automatic data transfer from the observation site to the Koganei campus of CRL, as well as for automatic data analysis and publication. Transfer of CRLFPI observation data is currently effected through this SALMON system.

3.3 Drive/Control System and House-keeping System

Step motors (Mellec Co. Ltd.) are used to adjust the mirror of the scanning FPI, the prism turret that guides the laser for calibration, the wavelength filter turret for acquisition of each channel, and the focus of the CCD camera. These parameters and sequences are controlled by the same workstation used for the image-retrieval system.

The housekeeping system consists of (1) a thermal-control unit to suppress temporal variations in the etalon gap, (2) a cooling-water circulation unit to cool the PCI, and (3) a dry-air circulation unit to prevent condensation on the PCI head. The temperature is constantly kept at 40 °C by (1), with heaters and thermostats. Unit (2) is controlled by the automatic observation system described in the next section.

3.4 Automatic Observation System

The basic principle of the automatic observation system is to manage the observation schedule with the PC by starting up the housekeeping system and the calibration lasers in the designated order at startup, and by shutting them down at the end of the observation period. This information is transmitted to the workstation as soon as the PC is ready for observation, and upon receiving the message, the workstation starts up the control programs for the drive/control system and the image-retrieval systems to begin data acquisition. At the end of observation, a message is sent from the PC to place the program in standby mode.

The reason behind this complex system lies in the fact that the automatic observation system was a later addition to a system originally designed for manual observation. Improvements are being made to simplify the system and to upgrade it into a more foolproof system. The new system, slated for implementation in the spring of 2003, will perform data retrieval, drive/control, and automatic observation from a single PC.

3.5 Data Analysis Software

The wind speed is determined from the change in fringe radius, assuming that the speed changes uniformly across the entire coverage in the scanning FPI observation. The S/N ratio can be improved by integrating once along the fringe circumference. However, slight imperfections in the installation of the optical systems may cause the fringe to deviate from a perfect circle. In such a case, corrections are made by referring to the shape

of the laser fringe before integration. This procedure is significantly more important for temperature estimations. When integration is performed without such correction, the fringe will have a wider form, resulting in estimations of higher-than-actual temperatures.

With all-sky FPI observation, each part of the fringe contains information concerning the wind and temperature for corresponding regions of the entire sky. In our analysis, to estimate the wind speed and temperature, each fringe is divided into 24 sectors with a center angle of 15°.

For both scanning and all-sky FPI observations, a standard reference point for a zero wind speed is required to calculate the absolute wind speed. Suggested methods for setting such a reference point include: (1) the use of data from cloudy days, when airglow is considered to be sufficiently affected by Mie scattering^[10]; (2) using the mean value of a single nighttime observation^{[11][12]}; or (3) performing fringe order conversion from laser fringes. Each of these methods has its advantages and drawbacks, and at present, there is no definitive method for the establishment of a standard reference point. Our present analysis adopts method (2).

Fig.7 shows the flow of the analysis software. This program performs automatic processing for the procedures listed above. This system is presently incorporated into SALMON and is set to perform a fully automatic analysis.

4 Example of Analysis

4.1 Thermospheric Vertical Winds in the Polar Regions

Vertical winds in the thermosphere in auroral zones with velocities sometimes exceeding 100 m/s, defying traditional predictions, have been observed and have begun to receive wide attention in recent years^[13]. Since vertical winds cause changes in the transfer of kinetic momentum and compositional structure of the atmosphere, they may significantly affect our understanding of the

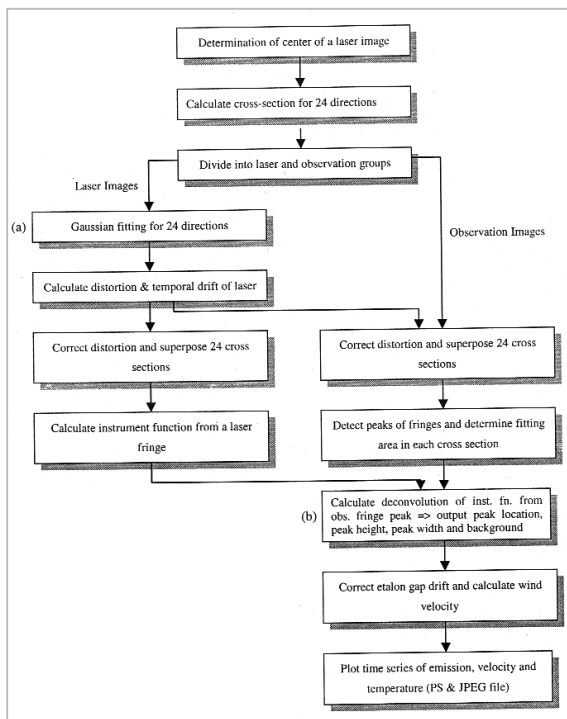


Fig.7 Flow of the analysis software

structure of the thermosphere[13].

The data presented here were collected from observations using the scanning CRLFPI at Poker Flat, Alaska, during the period from Oct. 1998 to Feb. 1999. The visible atomic oxygen emissions from the thermosphere (at 557.7 nm and 630.0 nm) were observed at a temporal resolution of two minutes. The auroral-luminance data in the geomagnetic N-S direction collected using the meridian scanning photometer (MSP) of UAF were treated as simultaneously observed data.

Fig.8 shows selected results. The horizontal and the vertical axis represent the elevation angle from the observation site and the intensity of the auroral luminosity at 557.7 nm, respectively. The auroral distribution during upward and downward winds observed by the CRLFPI differed significantly from the average of the entire data set. It was found that auroral luminosity decreases at the zenith and toward the pole during upward winds and increase toward the pole and decrease toward the equator during downward winds. This suggests the possibility that the wind system may change as a function of the position of the aurora[12].

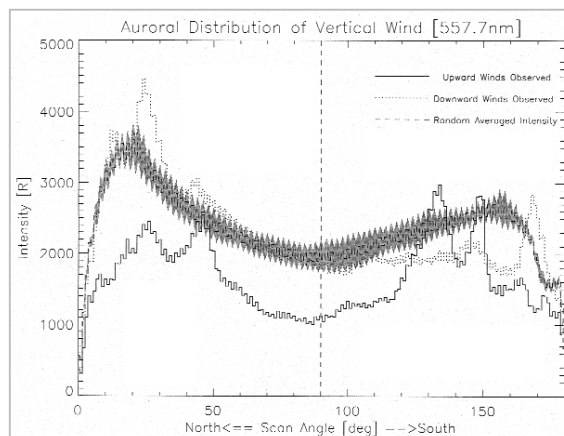


Fig.8 Correlation between the vertical wind and auroral position (statistical distribution)

Data are for 88 clear, nighttime skies between Sept. 1998 and Feb. 1999. Solid and dotted lines represent auroral distributions observed using the meridian scanning photometer (MSP) at the University of Alaska Fairbanks during observation of upward and downward winds, respectively. The dashed line and shaded area show the averages and the standard deviations of the aurora distribution on the hour for the same data set.

4.2 Interactions between Ionized and Neutral Particles

Above 100 km in the polar regions, there is a complex exchange of kinetic momentum between ionized and neutral atmospheres. In this region, a horizontal circulation of plasma is driven by the momentum of the high-speed plasma from the sun. Plasma constitutes only a small percentage (approximately 1%) of the atmosphere at an altitude of 250 km and constitutes approximately 0.01% at an altitude of 100 km. However, when a stable plasma flow persists for a certain amount of time, neutral winds are known to be driven by the ion drag. In addition, when there is a sudden change in the plasma flow (such as in a reversal of the interplanetary magnetic field), the delay in the motion of the neutral atmosphere causes a collision between the plasma and neutral winds, resulting in the generation of heat (the fly-wheel effect)[14].

Fig.9 shows the velocity vectors of neutral and ionized atmosphere observed simultaneously using the CRLFPI and the HF radar of the UAF and the University of Saskatchewan

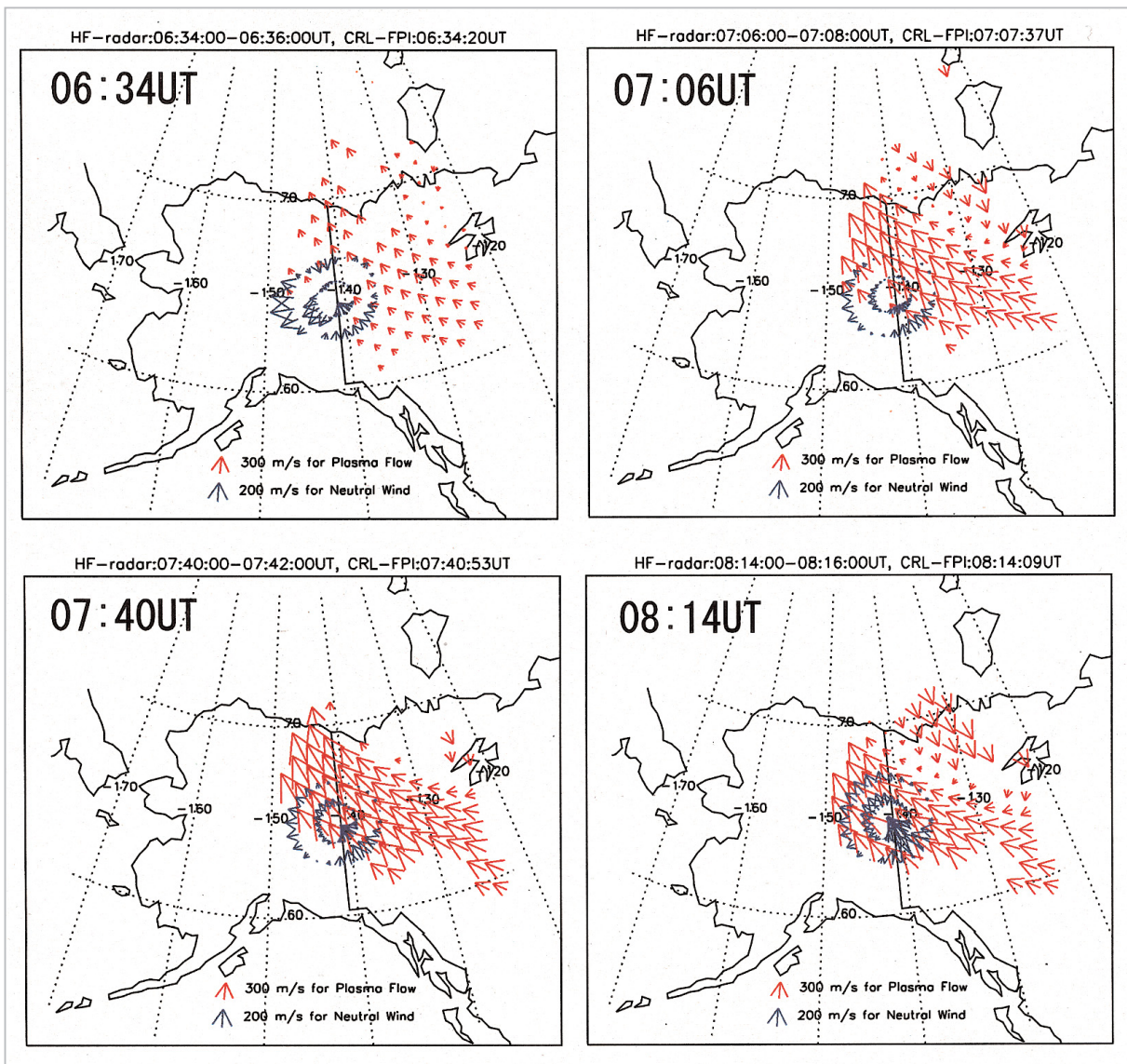


Fig.9 Variations in plasma flows and neutral winds observed on Nov. 24, 2000

Blue: Thermosphere vertical winds in the F region observed with CRLFPI; Red: Motions of the plasma flows observed with the HF radar at the University of Alaska Fairbanks and the University of Saskatchewan.

on Nov. 24, 2000. At 06:34 UT, neutral winds (blue) and plasma flow (red) featured vectors pointing to the west and northwest, respectively, but at 07:00 UT, the plasma flow began to accelerate in a stable manner in the northwest direction. In response to this acceleration, the neutral winds gradually began to shift to the northwest, picking up speed. At 08:46 UT, the speed of the plasma flow was 300 m/s, and the neutral winds had achieved a speed of nearly 180 m/s.

Conclusions

Development of the CRLFPI commenced in 1993, and after numerous collaborative observations in Japan, it was installed in Alaska in Sept. 1998 to begin continuous automatic observation.

The Fabry-Perot interferometer is generally considered to be an extremely difficult instrument to handle, due to the susceptibility of the etalon to temperature changes of the surrounding air, the susceptibility to damage of the PCI even at normal levels of visible

light, and other difficulties. The observation site selected must feature minimal artificial light, and specific measures to prevent dust and condensation on the various electronic devices are required. In this context, our efforts to develop a system for long-term automatic observation and to create software to retrieve wind-speed and temperature information may prove quite useful. In particular, satellite-borne Fabry-Perot interferometers such as the DE-2 (launched in 1981) have produced impressive results, and recent years have seen the development of more advanced instruments (such as UARS and TIMED). Regrettably, a satellite-borne FPI has yet to be developed in Japan, but we believe that with the progress of meteorological research, the significance of mesospheric and thermospheric

ic dynamics will be recognized, raising demand for FPI development. Against this background, CRL's development of its FPI should provide a foundation for such future development.

With respect to observations in Japan, we thank Prof. Hiroshi FUKUNISHI of Tohoku University and the staff at the Zao Observatory; Prof. Shoichiro FUKAO, Prof. Toshitaka TSUDA, Assoc. Prof. Takuji NAKAMURA, Assoc. Prof. Mamoru YAMAMOTO of Kyoto University, and the staff at the Shigaraki Observatory; (former) Director Kazumi NISHIMUTA of CRL and the staff at the Yamagawa Radio Observatory. For observations in Alaska, we are deeply grateful to June Perekowski, Brian Lawson, and Jerry Nelson.

References

- 1 Roble, R. G., and M. H. Rees, "Time-dependent studies of the aurora: Effects of particle precipitation on the dynamic morphology of ionospheric and atmospheric properties", *Planet. Space Sci.*, 25, 991-1010, 1977.
- 2 Rees, M. H., and J. C. G. Walker, "Ion and electron heating by auroral electric fields", *Ann. Geophys.*, 24, 193-198, 1968.
- 3 Killeen, T. L., P. B. Hays, and G. R. Carignan, "Ion-neutral coupling in the high-latitude F region: evaluation of ion heating terms from Dynamics Explorer 2", *J. Geophys. Res.*, 89, 7495-7508, 1984.
- 4 Lindzen, R. S., "Lower atmospheric energy sources for the upper atmosphere", *Meteor. Monogr.*, 9, 37-46, 1968.
- 5 Hernandez, G., *Fabry-Perot Interferometers*, "Cambridge studies in modern optics 3", Cambridge Univ. Press, p343, 1986.
- 6 Vaughan, J. H., "The Fabry-Perot Interferometer, history, theory, practice and applications", Adam Hilger, p583, 1989.
- 7 Ishii, M., S. Okano, E. Sagawa, S. Watari, H. Mori, I. Iwamoto, and Y. Murayama, "Development of Fabry-Perot interferometers for airglow observations", *Proc. NIPR. Symp. on Upper Atmos. Phys.*, 10, 97-108, 1997.
- 8 Ishii, M., S. Okano, E. Sagawa, S. Watari, H. Mori, I. Iwamoto, K. Kanda, F. Kamimura, and D. Sakamoto, "Development of an automatic observation system for Fabry-Perot interferometers", *Adv. Polar Upper Atmos. Res.*, 15, 178-192, 2001.
- 9 Oyama, S., Y. Murayama, M. Ishii, and M. Kubota, "Development of SALMON system and the environment data transfer experiment", This Special issue of CRL Journal.
- 10 Niihara, Y., *Doppler imaging observation of lower thermosphere wind at mid-latitude* (translated title), M.S. thesis, Tohoku University, Sendai Japan, 1994.
- 11 Ishii, M., S. Oyama, S. Nozawa, R. Fujii, E. Sogaqwa, S. Watari, and H. Shinagawa, "Dynamics of neutral wind in the polar region observed with two Fabry-Perot interferometers", *Earth Planet Space*, 51, 833-844, 1999.

- 12 Ishii, M., M. Conde, R. W. Smith, M. Krynicki, E. Sagawa and S. Watari, "Vertical wind observations with two Fabry-Perot interferometers at Poker Flat, Alaska", J. Geophys. Res., 106, 10537-10551, 2001.
- 13 Rees, D., R. W. Smith, P. J. Charleton, F. G. McCormac, N. Lloyd and A. Steen, "The generation of vertical thermospheric winds and gravity waves at auroral latitudes --- I. Observations of vertical winds", Planet. Space Sci., 32, 667-684, 1984.
- 14 Conde, M., and R. W. Smith, "Spatial structure in the thermospheric horizontal wind above Poker Flat, Alaska, during solar minimum", J. Geophys. Res., 103, 9449-9471, 1998.
- 15 Lyons, L. R., T. L. Killeen, and R. L. Waltercheid, "The neutral wind "flywheel" as a source of quiet-time, polar-cap currents", Geophys. Res. Lett., 101-104, 1985.



ISHII Mamoru, Dr. Sci.

Senior Researcher, International Arctic Environment Research Project Group, Applied Research and Standards Division

Atmospheric Dynamics

OKANO Syoichi, Dr. Sci.

Professor, Graduate School of Science, Tohoku University

Spectroscopy of Planetary and Terrestrial Upper Atmosphere

SAGAWA Eiichi, Dr. Sci.

Senior Researcher, Space Weather Group, Applied Research and Standards Division

Space Weather

MURAYAMA Yasuhiro, Ph. D.

Leader, International Arctic Environment Research Project Group, Applied Research and Standards Division

Observational Study of Middle Atmosphere



WATARI Shinichi, Dr. Sci.

Senior Researcher, Research Planning Office, Strategic Planning Division

Solar Terrestrial Physics

Mark Conde, Ph. D.

Assistant Professor of Physics, University of Alaska Fairbanks

Space Physics and Aeronomy

Roger W. Smith, Ph. D.

Director, Professor of Physics, University of Alaska Fairbanks

Upper-atmospheric Dynamics and Auroral Dynamics